JACS
JOURNAL OF THE AMERICAN CHEMICAL SOCIETY
Article
pubs.acs.org/JACS

Real-Time Observation of the Destruction of Hydration Shells under Electrochemical Force

Akira Yamakata,*[,†,‡] Eiji Soeta,[§] Tatsuya Ishiyama,[§] Masatoshi Osawa,[⊥] and Akihiro Morita*[,§,∥]

[†]Graduate School of Engineering, Toyota Technological Institute, 2-12-1 Hisakata, Tempaku, Nagoya 468-8511, Japan

[‡]Precursory Research for Embryonic Science and Technology (PRESTO), Japan Science and Technology Agency (JST), 4-1-8 Honcho Kawaguchi, Saitama 332-0012, Japan

[§]Department of Chemistry, Graduate School of Science, Tohoku University, Sendai 980-8578, Japan

[⊥]Catalysis Research Center, Hokkaido University, N-21 W-10, Kita-ku, Sapporo 001-0021, Japan

[∥]Elements Strategy Initiative for Catalysts and Batteries (ESICB), Kyoto University, Kyoto 615-8520, Japan

Supporting Information

ABSTRACT: Major alteration or even destruction of the hydration shell around interacting molecules and ions in solution is an important process that determines how hydrated substances interact. Therefore, the direct observation of structural changes in hydration shells around solutes in close contact with other solutes or surfaces is important for understanding chemical processes that take place in solution. In the work described in this paper, time-resolved IR absorption measurements were performed to study the interaction of hydrated Na^+ or tetrapropylammonium cation (Pr_4N^+) with a hydrophobic CO-covered Pt surface; the adsorption force between cations and the surface was controlled by using an electrochemical system. We found that the hydrophobic hydration shell of Pr_4N^+ is initially stabilized on the hydrophobic surface, but application of a strong force to the cation approaching CO destroys the water layers between them. This process is rather slow, taking a few hundred milliseconds. Hydrophilic Na^+ behaves quite differently from Pr_4N^+ due to the different structure of its hydration shell. These experimental results are supported by molecular dynamics simulations.

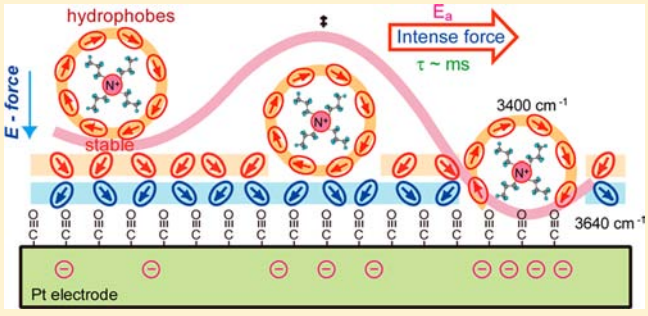

1. INTRODUCTION

Water molecules play essential roles in determining the behavior of molecules and ions in aqueous solutions.[1−3] Substances are stabilized in solutions by forming hydration shells. Structural changes of hydration shells perturb the energy state of solutes and hence affect their properties in solutions. Also, hydration shells physically prevent direct contact among the substances. Since any interaction among the substances is accompanied by a structural change in the water layers, it is important to study how the structures of hydration shells change when hydrated substances approach each other. This issue has been investigated in numerous theoretical works;[1−9] however, experiments are still very limited due to the experimental difficulties in controlling interactions between substances. Experimental verification of the theoretical predictions is indispensable to properly understand the real phenomena.

Vibrational spectroscopy is a powerful tool to study water molecules due to its high sensitivity to hydrogen bonding. Structures of water molecules around solutes and at interfaces under static conditions have been studied intensively by IR[10−12] and Raman[13−16] spectroscopies and vibrational sum-frequency generation (VSFG).[17−28] Moreover, time-resolved measurements and 2D-IR[29−32] have provided further information on the dynamics of water, such as orientation change,[33] vibrational relaxation,[30,34−38] and scission and formation of hydrogen-bonding.[25,28−32] Despite the progress of such advanced vibrational spectroscopy techniques, time-resolved study of the dynamics of the restructuring of hydration shells between hydrated substances is still very difficult because of the lack of triggering sources for synchronizing the measurement with the collision of hydrated substances.

In this work, we have overcome the experimental difficulties by combining an electrochemical system and surface-enhanced IR absorption spectroscopy (SEIRAS).[39] When cations are used as model solutes, they can accumulate immediately at the electrochemical interface upon rapidly shifting the electrode potential from −300 to −800 mV, negative from the potential of zero charge (pzc).[40] Furthermore, the interaction between the cation and the electrode surface can be controlled by varying the potential gradient at the interface: cations are pressed more strongly at more negative potentials, whereas

Received: April 30, 2013
Revised: August 22, 2013
Published: September 17, 2013

   dx.doi.org/10.1021/ja408326d | J. Am. Chem. Soc. 2013, 135, 15033−15039

anions are repelled from the surface. Time-resolved measurements with SEIRA configuration, which selectively probes the vicinity very near the surface,[39] enable observation of the rapid change of water structure between the ions and the surface at a time resolution ranging from picoseconds to seconds.[41] In the present work, structural changes of the hydration shells of Na^+ and tetrapropylammonium cation (Pr_4N^+) caused by their forced approach to a hydrophobic CO-covered Pt electrode were studied by time-resolved SEIRAS. We observed that the water layer on CO was immediately reconstructed upon the approach of hydrophilic Na^+, but it was hardly damaged by the approach of Pr_4N^+: a strong physical force exceeding a threshold and hundreds of milliseconds are required for the destruction of water layers, although the water layers among Pr_4N^+ and CO are constructed by simple hydrogen-bonding. The changes of free energy, enthalpy, and hydrogen-bonding structures were also evaluated by molecular dynamics (MD) simulations to confirm the results obtained by experiment.

2. EXPERIMENTAL SECTION

Time-resolved IR measurements were performed by using a homemade IR spectrometer, shown in Figure 1.[42] Briefly, the IR

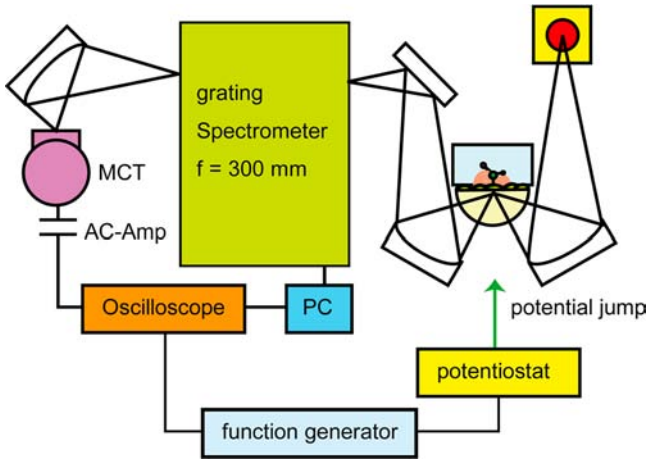

Figure 1. Diagram of the time-resolved IR absorption spectrometer for kinetic measurements on electrochemical processes.

light emitted from a $MoSi_2$ coil was focused on the reflection plane of the Si-ATR prism, and reflected light was detected by a photovoltaic MCT detector (Kolmar) after being monochromatized by a dispersive spectrometer (Acton SP-2300i). The output from the MCT was recorded in a digital oscilloscope (Iwatsu, DS-4262) as a function of delay time at a fixed wavenumber after the electrode potential was rapidly decreased from a reference potential of −300 mV to a sampling potential of −800 mV. The temporal profiles of the intensity change were reconstructed to transient IR absorption spectra at different delay times. The spectra were obtained with a resolution of 32 cm^{-1} in the O−H stretching region (4000−2900 cm^{-1}) and 16 cm^{-1} in the CO stretching and CH_3 deformation regions (2200−1400 cm^{-1}), and averaged over 10 scans for a spectrum. The time resolution of this spectrometer system is ∼20 ns, limited by the response of the MCT detector.

A Pt thin film prepared on a Si-ATR prism by a chemical deposition technique[43] was used as the working electrode. A double-jacket electrochemical cell with a Pt counter electrode and an Ag/AgCl (saturated KCl) reference electrode were used throughout the experiments. The temperature of the electrode and the solution was controlled by circulating temperature-controlled water in the outer jacket, while the reference electrode was thermally isolated from the cell and kept at 296 K to avoid temperature-dependent variation of its potential.

The electrode potential was controlled with a potentiostat (Hokuto Denko Co., HA-151A) and modulated with a function generator (NF circuit, WF1973) at 0.1 Hz. The reference potential was set to −0.3 V, while the sampling potential was changed from −0.4 to −0.9 V. During the experiments, no H_2 evolution was detected by cyclic voltammetry (Supporting Information, Figure S1). The potential range examined here is low enough relative the pzc (0.9 V for CO-covered Pt electrode[44]) that the effects of anions can be neglected. The absence of the effects of anions was also confirmed by using Br^- (NaBr and Pr_4NBr), Cl^- (Pr_4NCl), and SO_4^{2-} (H_2SO_4) instead of ClO_4^- ($NaClO_4$ and Pr_4NClO_4), as shown in Figures S2 and S3.

The electrode surface was cleaned by repeated electrochemical oxidation and reduction cycles in 0.5 M H_2SO_4. After being rinsed with Millipore water, the cell was quickly filled with aqueous solutions of 0.02 M tetrapropylammonium perchlorate (Pr_4NClO_4) or 0.1 M $NaClO_4$, prepared with Millipore water and research-grade chemicals purchased from Wako Chemicals. Pr_4NClO_4 was purified two times by recrystallization in ethanol. Before each experiment, the solution was deaerated with Ar and then CO. Experiments were performed in the presence of dissolved CO.

3. RESULTS AND DISCUSSION

3.1. CO-Covered Pt Electrode and Its Response to the Negative Potential Jump. In this work, we used a CO-covered Pt electrode because CO strongly adsorbs on the Pt electrode at negative potentials and provides a stable model hydrophobic surface on which to examine the behavior of water molecules. As we reported previously,[11] covering the surface with CO weakens the interaction between the cations and the surface and delays the destruction of hydration shells of cations, to facilitate examination of the process by which they are destroyed. Furthermore, the adsorbed CO serves as a probe to monitor the change of the electrode potential with respect to the externally applied potential perturbation, because the C−O stretching vibration is proportional to the actual electrode potential and responds to it in the picosecond region.[41]

The time-resolved SEIRA spectra of adsorbed CO for a potential jump from −0.3 to −0.8 V in $NaClO_4$ solution are shown in Figure 2A. The spectra exhibit a bipolar-shaped feature composed of a negative peak at 2070 cm^{-1} and a positive peak at 2045 cm^{-1}. Since CO is neither desorbed nor oxidized in this potential range, the bipolar shape is ascribed to the red-shift of on-top CO caused by the so-called "Stark tuning effects" and/or electron back-donation from the surface to the $2\pi^*$ orbital of CO.[45] Independent measurements with and without adsorbed CO showed that the peak frequency is 2062 cm^{-1} at −0.3 V and 2047 cm^{-1} at −0.8 V.[12] The intensity of the negative peak is approximately proportional to the shift of the vibrational frequency,[46] and hence it is correlated with the electrode potential. From the temporal profile of the intensity at 2070 cm^{-1} shown in Figure 2C (upper trace), the time constant of the potential shift, i.e., the time constant of the double-layer charging, τ_{dl} ($= R_{cell}C_{dl}$), is estimated to be 3 ms, where R_{cell} and C_{dl} are the cell resistance and double-layer capacitance, respectively. Since the actual potential at the interface is given as $E(t) = E_{ini} + \Delta E \exp(-t/\tau_{dl})$,[46] the time resolution of this potential-jump-coupled SEIRAS is limited to be a few milliseconds, although the spectrometer itself has a 20 ns time resolution.

3.2. Structural Changes of Water Layers on CO-Covered Pt Surface upon the Approach of Hydrated Na^+. The negative potential jump induces structural changes of water layers on CO-covered Pt electrodes. As shown in Figure

dx.doi.org/10.1021/ja408326d | J. Am. Chem. Soc. 2013, 135, 15033−15039

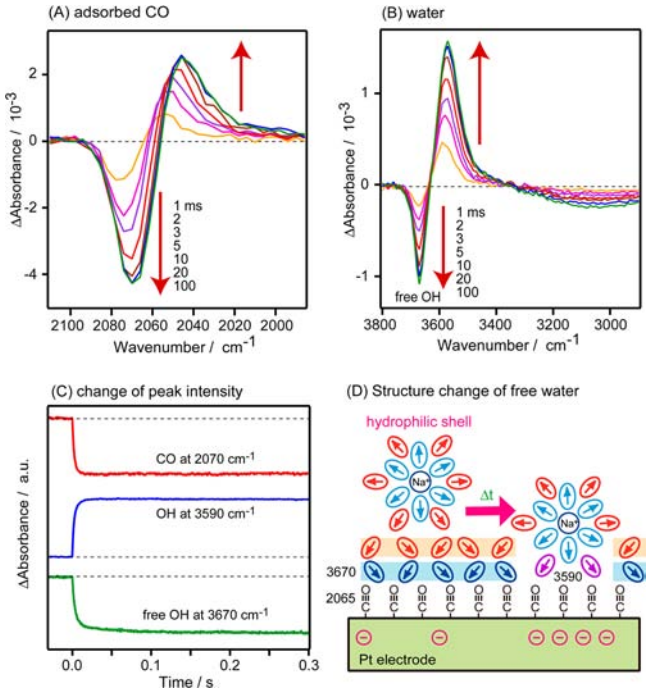

Figure 2. Time-resolved IR spectra of a CO-covered Pt electrode in 0.1 M Na^+-containing solution. The difference by the potential jump from −300 to −800 mV vs Ag/AgCl is shown. (A) Adsorbed CO on Pt (2062 cm^{-1}) and (B) water on CO (3670 cm^{-1}). (C)Temporal profiles of these band intensities. (D) Schemes of structure change of free water on CO upon the approach of hydrated Na^+.

2B, the band intensity at 3670 cm^{-1} rapidly decreased, and a new band appeared at 3590 cm^{-1} within 20 ms. As reported in our previous publications,[11,12] the 3670 cm^{-1} band is assigned to H-bonding free water molecules directing an O−H bond to CO (this water is termed hereafter as free water). A similar band has always been observed at hydrophobic interfaces such as air/water,[17] water/hexane,[18] and water/CCl_4,[19] and hence this band is often used as an indicator to examine the hydrophobicity of the interface.

The time constant of the decrease of the 3670 cm^{-1} band and increase of the 3590 cm^{-1} band is estimated to be 3 ms from Figure 2C (middle and lower traces), as is the case for CO vibration. Since cations are accumulated at the interface within this time scale, as will be shown later, the new band appearing at 3590 cm^{-1} can be ascribed to water molecules interacting with both Na^+ and CO; the red-shift of ∼80 cm^{-1} from the free OH band (3670 cm^{-1}) is likely induced by hydrogen-bonding with the hydration shell of Na^+. The similar red-shift of the free OH band was observed in hydrophilic cations such as Mg^{2+}, Zn^{2+}, and Me_4N^+.[12] Although the band intensity at 3400−3000 cm^{-1} was slightly decreased, no drastic changes were observed in these regions, where the hydration shell of Na^+ is expected to give a broad band characteristic of hydrogen-bonded water.[47] Since the accumulation of hydrated Na^+ should repel the water molecules that existed at the interface before, the result suggests that the spectrum of the hydration shell at 3400−2900 cm^{-1} is very similar to that of bulk water, and that the both contributions (removal of water at the interface and increase of the hydration shell of Na^+) are canceled out by taking the potential difference.

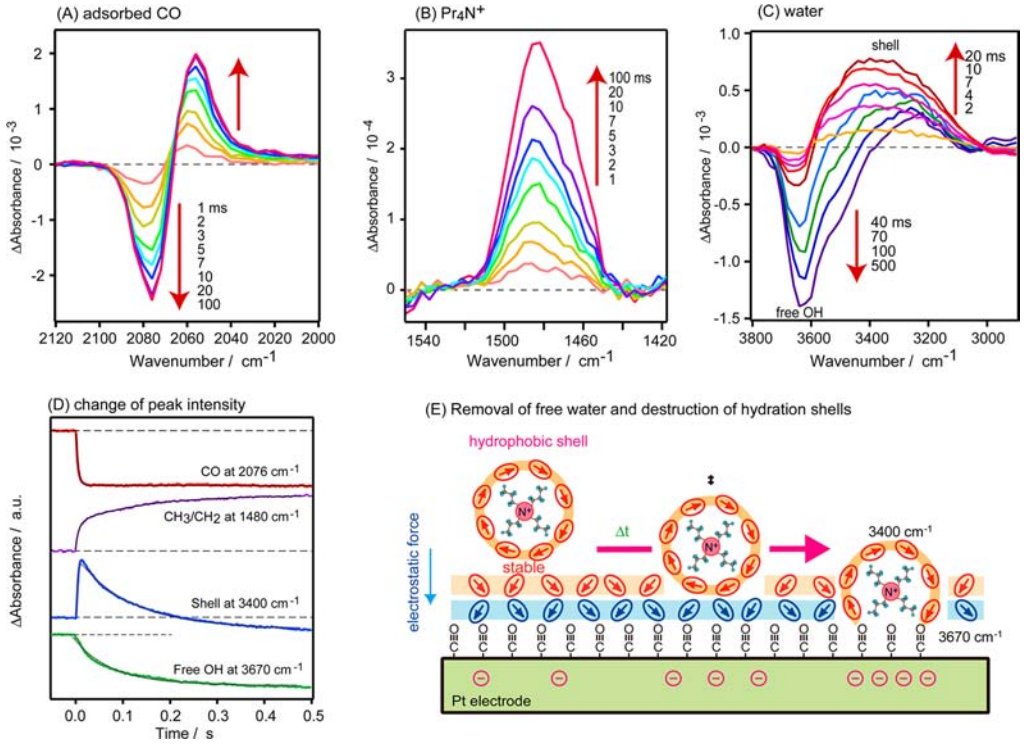

Figure 3. Time-resolved IR spectra of a CO-covered Pt electrode in 0.02 M Pr_4N^+-containing solution. The difference upon the potential jump from −300 to −800 mV vs Ag/AgCl is shown. (A) Adsorbed CO on Pt (2070 cm^{-1}), (B) CH_3/CH_2 of Pr_4N^+, (C) water of hydration shell around Pr_4N^+ (3400 cm^{-1}), and free OH on CO (3670 cm^{-1}) are shown. (D) Temporal profiles of these band intensities. (E) Schemes of removal of free water on CO and destruction of the hydration shell.

dx.doi.org/10.1021/ja408326d | J. Am. Chem. Soc. 2013, 135, 15033−15039

3.3. Accumulation and Destruction of Hydrated Pr_4N^+ at the CO-Covered Pt Surface. The same experiments were performed by using Pr_4NClO_4 as the supporting electrolyte. As is the case with Na^+, the frequency of the adsorbed CO is red-shifted by the negative potential jump (Figure 3A). The time constant of the double-layer charging is estimated to be 5 ms from the transient of the intensity at 2078 cm^{-1} (Figure 2D), in accordance with the experiment using $NaClO_4$.

The potential jump to the negative direction induces a more negative charge on the electrode surface, and hence should increase the concentration of cations (Pr_4N^+) at the interface. In fact, the accumulation of Pr_4N^+ is clearly demonstrated in the 1550−1420 cm^{-1} region (Figure 3B). The band at 1480 cm^{-1} that develops with time is undoubtedly assigned to the asymmetric CH_3 deformation and/or CH_2 deformation of Pr_4N^+; the two modes cannot be distinguished in the present case due to the low spectral resolution employed. The intensity at 1480 cm^{-1} increases in two steps: an initial very fast step with a time constant of 5 ms and a subsequent slow step with a time constant of 180 ms (Figure 3D). The time constant of the initial component is identical to that of the frequency shift of CO (i.e., doudle-layer charging), and hence it can be ascribed to the increase in the concentration of Pr_4N^+ at the interface. On the other hand, the time constant of the second slow increase of the band intensity is identical to that of the destruction of the hydration shell of Pr_4N^+, as will be shown later. The absorption intensity of Pr_4N^+ depends not only on its concentration but also on its distance from the surface, since the SEIRA effect sharply decreases with the distance from the surface.[39] Destruction of the hydration shell lets the cation closer to the surface; therefore, the second slow increase of the band intensity will be related to the destruction of the hydration shell.

Concomitant with the accumulation of Pr_4N^+ at the interface, a broad band centered at ∼3400 cm^{-1} appears and grows with time, accompanied by a slight decrease of the band at 3640 cm^{-1}. The time constant of the initial increase (up to 20 ms) is estimated to be 5 ms, which is identical to those of double-layer charging and the accumulation of Pr_4N^+ at the interface. The increase of the broad band at ∼3400 cm^{-1} has been observed commonly in solutions of hydrophobic cations such as Et_4N^+, Pr_4N^+, and Bu_4N^+, but not in the solutions of hydrophilic cations such as Na^+, Mg^{2+}, Zn^{2+}, and Me_4N^+.[11,12] Accordingly, this band is assigned to the hydrophobic hydration shell around the Pr_4N^+. This assignment is consistent with the IR study of hydration shells around various hydrophobic R_4N^+ in bulk water.[47,48] The accumulation of hydrated Pr_4N^+ should repel the water molecules that existed at the interface before, but the negative band of the repelled water is not identified in the spectra from 3400 to 2900 cm^{-1}. In fact, the spectrum of the hydration shell around R_4N^+ is very similar to that of the bulk water,[47,48] but the density of water is different. Water molecules around R_4N^+ are more structured than in the bulk, and hence its density is higher.[49,50] Therefore, the approach of Pr_4N^+ increases the density of water at the interface and increases the band intensity of H-bonded water at around 3400 cm^{-1}.

Interestingly, drastic changes occur in the OH stretching region of the hydration shell at 20−40 ms after the negative potential jump (Figure 3C). The characteristic band of the free water at ∼3640 cm^{-1} significantly reduces its intensity with time, accompanied by a negative broad shoulder at about 3500 cm^{-1}. The result strongly suggests that the free water on CO is removed and the hydration shell around Pr_4N^+ is destroyed, with a significant rearrangement of water molecules at the interface. Similar results were observed in the potential-sweeping FT-IR measurements. In the case of Pr_4N^+ and Bu_4N^+, destruction of hydration shells and the removal of free water on CO take place, but only the removal of free water occurs by the approach of Et_4N^+.[11] The destruction of the hydration shell depends on the property of the cations.

Although, the spectral changes of the O−H region are complex and seems difficult to determine their actual shapes and peak frequencies, the sharp negative peak at 3640 cm^{-1} is well separated from the broad positive peak at 3400 cm^{-1}. Therefore, the intensities at 3670 and 3400 cm^{-1} will be a good measure to analyze the change of free water and hydration shell, respectively. The intensity transients at the two wavenumbers are shown in Figure 3D, and the time constants of the destruction of the hydration shell and the removal of free water on CO are estimated to be 185 and 170 ms, respectively. These results suggest that the destruction of the hydration shell proceeds simultaneously with the removal of free water on top of CO: these two processes are not independent of each other.

3.4. Kinetic Analysis of the Destruction of Hydration Shells around Pr_4N^+. In order to study the destruction processes in detail, kinetic analysis was performed. Since the driving force for the destruction of the hydration shell is thought to be the electrostatic force on the cations toward the surface, the rate of hydration shell destruction is expected to depend on the applied potential. To confirm this assumption, the potential was stepped from −0.3 V to a value in the range of −0.4 to −0.9 V (Figure 4A). For the potential jump down to −0.5 V, the intensity at 3400 cm^{-1} (the OH stretching band of hydration shell) rapidly increases after the potential jump due to the accumulation of Pr_4N^+ and then remains constant, while the intensity of free water on CO (3670 cm^{-1}) keeps constant. These results indicate that neither the destruction of the hydration shell nor the removal of free water on CO occurs in this potential range, and suggest that the hydration shell and free water on CO have sufficient mechanical persistence against the force applied to Pr_4N^+ toward the surface under this condition.

When the negative potential is increased from −0.5 to −0.9 V, the intensities at the two wavenumbers start to decrease after 40 ms due to the destruction of the hydration shell and the removal of free water. The decrease of the intensities is more significant and faster at more negative potentials. The rate constants (k) of the two processes estimated from Figures 4A are plotted in Figure 4B as a function of the applied potential. Since the force on the cations toward the surface becomes intense at more negative potentials, this figure clearly demonstrates that the force directing the cation toward the surface is responsible for the restructuring of water molecules between the cation and CO. The removal of free water is slightly slower than the destruction of the hydration shell, which may reflect the difference in the hardness of water layers: it is known that stronger hydrophobic hydration shells are formed on smaller molecules than on flat surfaces.[5]

To gain further insight into the destruction kinetics, the temperature dependence of the rate constants was examined. As the temperature becomes higher, both of the rates become faster (Figure 4C). From the data, the activation energies for the destruction of hydration shells and the removal of free water layers are estimated to be 7.3 ± 0.5 and 7.0 ± 0.5 kJ mol^{-1}, respectively, which are independent of the applied potential in the range of −0.7 to −0.9 V (Figure 4D). The very

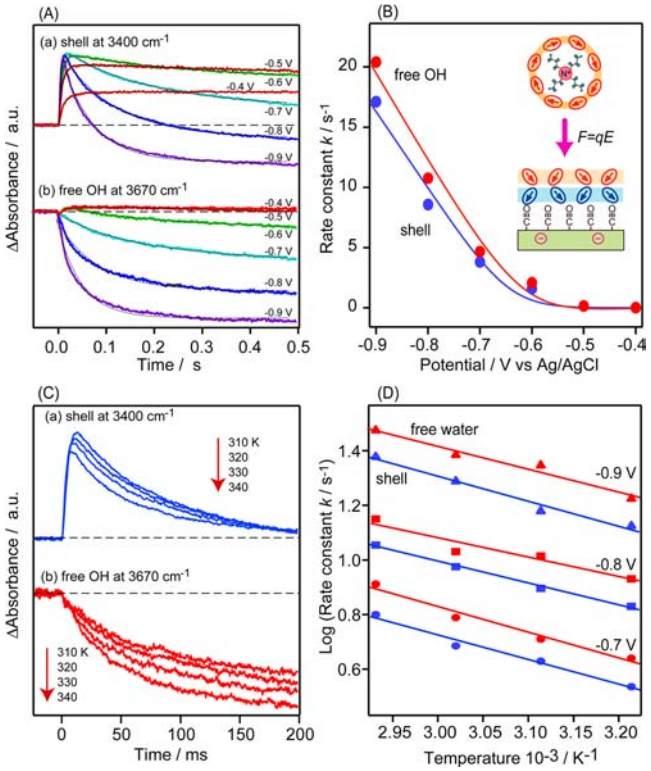

Figure 4. Kinetic analysis of destruction of the hydration shell around Pr_4N^+ and removal of free water on CO. (A) Potential-dependent temporal profiles of band intensities at 3400 and 3670 cm^{-1}. These curves were measured at 310 K by the potential jump from −0.3 to the indicated potentials. (B) Potential-dependent rate constants of the destruction processes. (C) Temperature-dependent temporal profiles of band intensities at 3400 and 3670 cm^{-1}. These curves were measured by the potential jump from −0.3 to −0.8 V at the indicated temperatures. (D) Arrhenius plots for removal of free water (red plots) and destruction of the hydration shells (blue plots) measured at −0.7, −0.8, and −0.9 V.

similar activation energies also suggest that the two processes take place simultaneously.

3.5. Molecular Dynamics Simulations. For further understanding, the behavior of water molecules upon the approach of Pr_4N^+ to the CO-covered Pt surface was studied by MD simulations. Figure 5A shows the calculated free energy change during the approach of Pr_4N^+ to the CO-covered Pt surface. The energy is plotted as a function of the distance of the cation to the center of mass of the oxygen atom of CO. As shown in the figure, there are two energy local minima, A and B (at ∼13 and 4.5 Å, respectively), and one local maximum, at 9 Å. The local minimum B (4.5 Å) is due to the stabilization of Pr_4N^+ by its direct contact with hydrophobic CO. The distance of the shallow local minimum A (13 Å) suggests the presence of a few water molecules between Pr_4N^+ and CO. It is worth noting that such a local minimum has been observed around several molecules, such as CH_4,[2,3] neopentane,[8] and C_{60},[7] and the formation of a water-inserted structure represented as hydrophobe−$(water)_n$−hydrophobe has been proposed. The present simulation is consistent with these molecular systems. On the other hand, the local energy maximum (transition state) at 9 Å suggests the necessity of an activation energy for the destruction of water layers between Pr_4N^+ and CO. The difference of free energy between the transition state and the bulk (13 Å) was estimated to be 1.7 kJ mol^{-1} from Figure 5A, and the activation energy was estimated to be 6.2 kJ mol^{-1} by calculating the enthalpy change of the system. The activation energy predicted by MD simulation is in good agreement with the experiment (∼7 kJ mol^{-1}).

In order to obtain more detailed pictures of the structural change of water molecules, the spatial distribution of the hydrogen bond, $\Delta N = N(\text{donor}) - N(\text{acceptor})$, was calculated, where N(donor) and N(acceptor) are the numbers of hydrogen-donating and -accepting OH bonds. In Figure 5C, the acceptor-rich ($\Delta N < 0$) and donor-rich ($\Delta N > 0$) regions are colored in blue and red, respectively. This figure shows that hydrophobic hydration shells around Pr_4N^+ consist of donor-rich water, and that the water layers on CO have a structure in which acceptor-rich and donor-rich water layers are piled up alternatingly. Since CO is hydrophobic, the first water layer is acceptor-rich: this result is consistent with the experimental observation of the "free OH" band at 3670−3640 cm^{-1}. It is noted that the acceptor-rich first layer is stabilized by the donor-rich second layer. On the other hand, the hydration shell of Pr_4N^+ is stabilized by the strong hydrogen-bonds among water molecules to form iceberg- or clathrate-like cages.[2,3]

Here, we see how the water layers on CO are affected by the approach of Pr_4N^+ from the bulk. When Pr_4N^+ reaches the first minimum, point A, at 13 Å, the third weakly structured water layer on CO is removed first. As the distance between Pr_4N^+ and CO becomes shorter down to 9 Å, the second water layer on CO is removed and the free energy increases due to the destabilization of the first layer. Note once again that the hydration shell of Pr_4N^+ is formed by water molecules strongly hydrogen-bonded to each other. Therefore, the hydrophobic hydration shells of Pr_4N^+ cannot donate their hydrogen bonds to stabilize the first free water layer on CO. After the second water layer is completely removed (transition state), the hydration shell around Pr_4N^+ contacts with the first water layers on CO, and the destruction of the hydration shell and the removal of the first free water layer proceed simultaneously to make their direct contact. The results suggest that the removal of the second water layer on CO governs the destruction processes of the hydrophobic hydration shells around Pr_4N^+, as sketched in Figure 3E.

However, in the case of hydrophilic Na^+, the simulated result is largely different from that for hydrophobic Pr_4N^+, as shown in Figure 5B,D. The most striking difference is the structures of the hydration shells around the two cations. The primary shell around Na^+ is donor-rich, as is the case with Pr_4N^+, but an acceptor-rich secondary shell is formed, suggesting that water molecules in the primary shell orient their OH bonds outward. Owing to this structure, hydrated Na^+ at 8−10 Å can remove the second water layer on CO without changing the free energy by donating OH bonds to the first acceptor-rich layer. A very shallow minimum appears at 8 Å in the energy profile (Figure 5B). At shorter distances down to 5 Å, Na^+ additionally removes the first water layer on CO, which results in a slight increase of the free energy. During this process, the acceptor-rich secondary shell of Na^+ merges with the acceptor-rich first water layer on CO. As a result, it becomes difficult to distinguish them. Destruction of the primary shell drastically increases the free energy (at <5 Å). As long as the destruction of the primary shell does not occur, a structure at 6−8 Å shown in Figure 5D is likely to be formed in the real system, depending on the applied potential. In this case, the first water layer on CO remains, and the hydrated Na^+ is in close contact

dx.doi.org/10.1021/ja408326d | J. Am. Chem. Soc. 2013, 135, 15033−15039

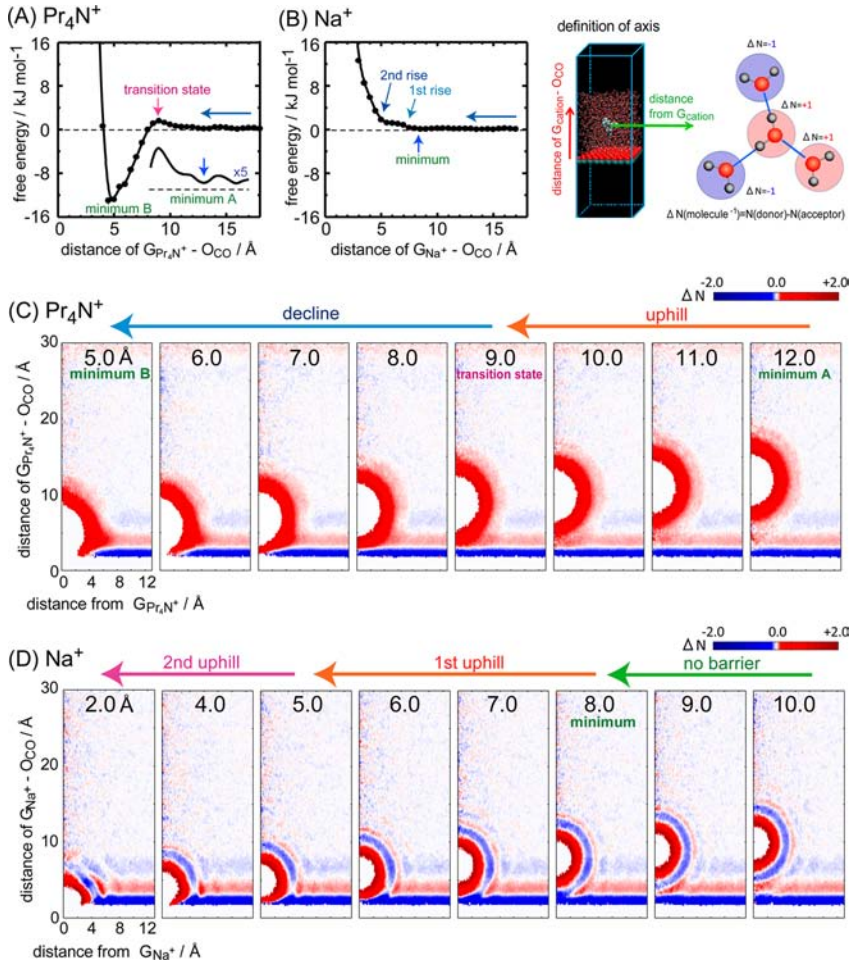

Figure 5. MD simulated change of free energy during the approach of Pr_4N^+ (A) and Na^+ (B) toward the CO-covered Pt electrode. The energy is plotted as a function of the distance between the center of mass of the cation (Pr_4N^+ or Na^+) and the oxygen atom of CO. MD simulated spatial distribution of donor-rich and acceptor-rich regions of water molecules at the interface during the approach of Pr_4N^+ (C) and Na^+ (D) toward the CO-covered Pt electrode. The red and blue regions show donor-rich and acceptor-rich regions defined by $\Delta N(\text{molecule}^{-1}) = N(\text{donor}) - N(\text{acceptor})$.

with it, which well explains the potential-dependent shift of the OH stretching band of free water shown in Figure 2B.

4. CONCLUSION

In this work, we observed the structural change of water molecules during close contact of hydrated cations (Na^+ and Pr_4N^+) to the hydrophobic CO-covered Pt electrode surface by using time-resolved IR absorption spectroscopy with the potential jump method. The reconstruction of water layers depends on the hydrophobicity of the cation and applied potential. The hydration shell of hydrophilic Na^+ is rigid and hardly destroyed at the interface, while the hydration shell of hydrophobic Pr_4N^+ is destroyed, and the cation directly contacts with CO by removing the water layer on CO. The different behaviors of cations arise from the different structures of their hydration shells. The rearrangement of water molecules is induced by the forced approach of the cations toward the surface in the strong electric field at the electrochemical interface, and so its rate depends on the applied potential. The activation energy of the rearrangement for Pr_4N^+ was estimated to be ~7 kJ mol^{-1}. MD simulation of water molecules at the interface was in good accordance with the experiments.

■ ASSOCIATED CONTENT

Supporting Information

Cyclic voltammetry, potential-sweeping FT-IR measurements, effects of anions, and details of MD simulations. This material is available free of charge via the Internet at http://pubs.acs.org.

■ AUTHOR INFORMATION

Corresponding Authors

yamakata@toyota-ti.ac.jp
morita@m.tohoku.ac.jp

Notes

The authors declare no competing financial interest.

■ ACKNOWLEDGMENTS

This work was partly supported by JSPS KAKENHI Grant Nos. 23360360 and 24550143, and Priority Areas 477.

■ REFERENCES

(1) Frank, H. S.; Evans, M. W. *J. Chem. Phys.* **1945**, *13*, 507.
(2) Blokzijl, W.; Engberts, J. *Angew. Chem., Int. Ed.* **1993**, *32*, 1545.
(3) Southall, N. T.; Dill, K. A.; Haymet, A. D. J. *J. Phys. Chem. B* **2002**, *106*, 521.
(4) Mucha, M.; Frigato, T.; Levering, L. M.; Allen, H. C.; Tobias, D. J.; Dang, L. X.; Jungwirth, P. *J. Phys. Chem. B* **2005**, *109*, 7617.

(5) Lee, C. Y.; McCammon, J. A.; Rossky, P. J. *J. Chem. Phys.* **1984**, *80*, 4448.
(6) Jungwirth, P.; Tobias, D. J. *J. Phys. Chem. B* **2002**, *106*, 6361.
(7) Hotta, T.; Kimura, A.; Sasai, M. *J. Phys. Chem. B* **2005**, *109*, 18600.
(8) Thomas, A. S.; Elcock, A. H. *J. Am. Chem. Soc.* **2007**, *129*, 14887.
(9) Ishiyama, T.; Morita, A. *J. Phys. Chem. C* **2007**, *111*, 721.
(10) Ataka, K.; Yotsuyanagi, T.; Osawa, M. *J. Phys. Chem.* **1996**, *100*, 10664.
(11) Yamakata, A.; Osawa, M. *J. Am. Chem. Soc.* **2009**, *131*, 6892.
(12) Yamakata, A.; Osawa, M. *J. Phys. Chem. Lett.* **2010**, *1*, 1487.
(13) Green, J. L.; Sceats, M. G.; Lacey, A. R. *J. Chem. Phys.* **1987**, *87*, 3603.
(14) Perera, P. N.; Browder, B.; Ben-Amotz, D. *J. Phys. Chem. B* **2009**, *113*, 1805.
(15) Davis, J. G.; Gierszal, K. P.; Wang, P.; Ben-Amotz, D. *Nature* **2012**, *491*, 582.
(16) Rankin, B. M.; Hands, M. D.; Wilcox, D. S.; Fega, K. R.; Slipchenko, L. V.; Ben-Amotz, D. *Faraday Discuss.* **2013**, *160*, 255.
(17) Du, Q.; Superfine, R.; Freysz, E.; Shen, Y. R. *Phys. Rev. Lett.* **1993**, *70*, 2313.
(18) Du, Q.; Freysz, E.; Shen, Y. R. *Science* **1994**, *264*, 826.
(19) Scatena, L. F.; Brown, M. G.; Richmond, G. L. *Science* **2001**, *292*, 908.
(20) Sovago, M.; Campen, R. K.; Wurpel, G. W. H.; Muller, M.; Bakker, H. J.; Bonn, M. *Phys. Rev. Lett.* **2008**, *100*, 173901.
(21) Shultz, M. J.; Baldelli, S.; Schnitzer, C.; Simonelli, D. *J. Phys. Chem. B* **2002**, *106*, 5313.
(22) Raymond, E. A.; Richmond, G. L. *J. Phys. Chem. B* **2004**, *108*, 5051.
(23) Gopalakrishnan, S.; Liu, D. F.; Allen, H. C.; Kuo, M.; Shultz, M. J. *Chem. Rev.* **2006**, *106*, 1155.
(24) Ostroverkhov, V.; Waychunas, G. A.; Shen, Y. R. *Phys. Rev. Lett.* **2005**, *94*, 4.
(25) Stiopkin, I. V.; Weeraman, C.; Pieniazek, P. A.; Shalhout, F. Y.; Skinner, J. L.; Benderskii, A. V. *Nature* **2011**, *474*, 192.
(26) Tian, C. S.; Shen, Y. R. *Proc. Natl. Acad. Sci. U. S. A.* **2009**, *106*, 15148.
(27) Nihonyanagi, S.; Ishiyama, T.; Lee, T.; Yamaguchi, S.; Bonn, M.; Morita, A.; Tahara, T. *J. Am. Chem. Soc.* **2011**, *133*, 16875.
(28) Singh, P. C.; Nihonyanagi, S.; Yamaguchi, S.; Tahara, T. *J. Chem. Phys.* **2012**, *137*, 6.
(29) Fecko, C. J.; Eaves, J. D.; Loparo, J. J.; Tokmakoff, A.; Geissler, P. L. *Science* **2003**, *301*, 1698.
(30) Asbury, J. B.; Steinel, T.; Stromberg, C.; Corcelli, S. A.; Lawrence, C. P.; Skinner, J. L.; Fayer, M. D. *J. Phys. Chem. A* **2004**, *108*, 1107.
(31) Kraemer, D.; Cowan, M. L.; Paarmann, A.; Huse, N.; Nibbering, E. T. J.; Elsaesser, T.; Miller, R. J. D. *Proc. Natl. Acad. Sci. U.S.A.* **2008**, *105*, 437.
(32) Roberts, S. T.; Ramasesha, K.; Tokmakoff, A. *Acc. Chem. Res.* **2009**, *42*, 1239.
(33) Omta, A. W.; Kropman, M. F.; Woutersen, S.; Bakker, H. J. *Science* **2003**, *301*, 347.
(34) Woutersen, S.; Bakker, H. J. *Nature* **1999**, *402*, 507.
(35) Kropman, M. F.; Bakker, H. J. *J. Am. Chem. Soc.* **2004**, *126*, 9135.
(36) Ghosh, A.; Smits, M.; Bredenbeck, J.; Bonn, M. *J. Am. Chem. Soc.* **2007**, *129*, 9608.
(37) Eftekhari-Bafrooei, A.; Borguet, E. *J. Am. Chem. Soc.* **2009**, *131*, 12034.
(38) Eftekhari-Bafrooei, A.; Borguet, E. *J. Am. Chem. Soc.* **2010**, *132*, 3756.
(39) Osawa, M. *Bull. Chem. Soc. Jpn.* **1997**, *70*, 2861.
(40) Bockris, J. O. M.; Reddy, A. K. N.; Gamboa-Aldeco, M. *Modern Electrochemistry*, 2nd ed.; Kluwer Academic/ Plenum Publishers: New York, 2000.
(41) Yamakata, A.; Uchida, T.; Kubota, J.; Osawa, M. *J. Phys. Chem. B* **2006**, *110*, 6423.
(42) Yamakata, A.; Yoshida, M.; Kubota, J.; Osawa, M.; Domen, K. *J. Am. Chem. Soc.* **2011**, *133*, 11351.
(43) Miki, A.; Ye, S.; Osawa, M. *Chem. Commun.* **2002**, 1500.
(44) Cuesta, A. *Surf. Sci.* **2004**, *572*, 11.
(45) Nichols, R. J. *Adsorption of Molecules at Metal Electrodes*; VCH: New York, 1992.
(46) Laane, J.; Kiefer, W. *J. Chem. Phys.* **1980**, *72*, 5305.
(47) Stangret, J.; Gampe, T. *J. Phys. Chem. A* **2002**, *106*, 5393.
(48) Pieniazek, P. A.; Stangret, J. *Vib. Spectrosc.* **2005**, *39*, 81.
(49) Lee, I.; Hyne, J. B. *Can. J. Chem.* **1968**, *46*, 2333.
(50) Hirata, F.; Arakawa, K. *Bull. Chem. Soc. Jpn.* **1973**, *46*, 3367.